Answers

1.

A function that would shift an array by an arbitrary amount using a convolution was constructed such that it would take two arguments – an array and an amount by which to shift the given array. A Gaussian started in the center of the array was utilized to show the function's operation. It was shifted by half the array length (Figure 1).

2.

a)

The correlation function utilizing Fourier Transform (FT) functions was studied:

$$f \bigstar g = \text{ift}(\text{dft}(f)^*\text{conj}(\text{dft}(g))$$

A routine was written to take the correlation function of two arrays. The Gaussian from Q1 was adopted. Figure 2 shows the correlation function of the Gaussian with itself. The correlation of a Gaussian with itself would have the same profile of the Gaussian, as evidenced by the plot.

b)

Results of part (a) helped build another routine to determine the correlation function of a Gaussian (shifted by an arbitrary amount) with itself. Shifts of several array lengths were examined (Figure 3). The correlation function profile was identical to the Gaussian itself, albeit with wrapping around; it was simply translated by the shift amount. These results were not surprising because the correlation of a Gaussian with itself, shifted or not, should produce identical curves. The effect of shift would then be reflected in the distance between the initial and shifted curves along the x axis.

3.

Given the challenges posed by the circulant nature of the dft in analysis, a routine was explored to take an FFT-based convolution of two arrays of length m and n, avoiding wrap-around. Zeros were added to the end of input arrays to achieve padded arrays of length $m+n-1$. Resultant correlation data points were compared to those output by the in-built np.convolve function; a good agreement therein was observed (Figure 4).

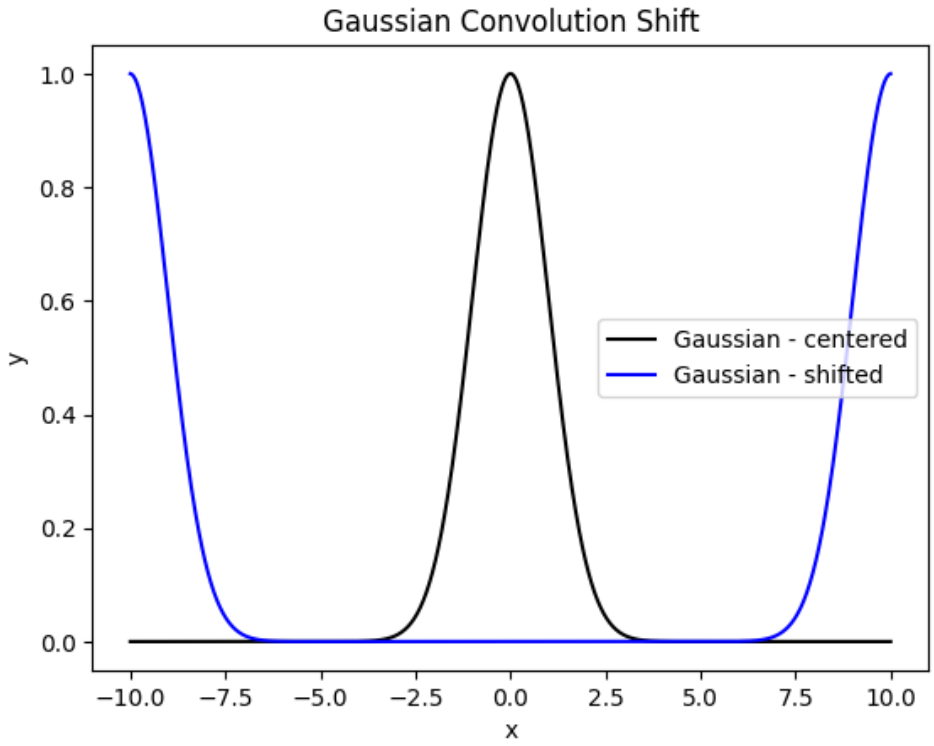

Figure 1. Array-centered gaussian shifted by half array length

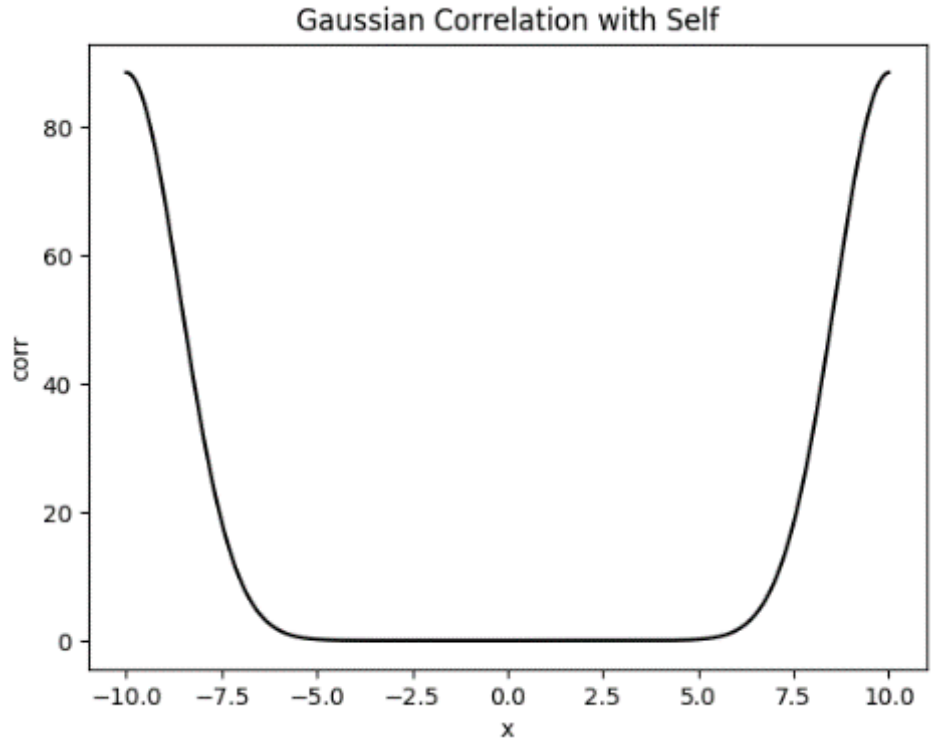

Figure 2. Correlation of a Gaussian with itself

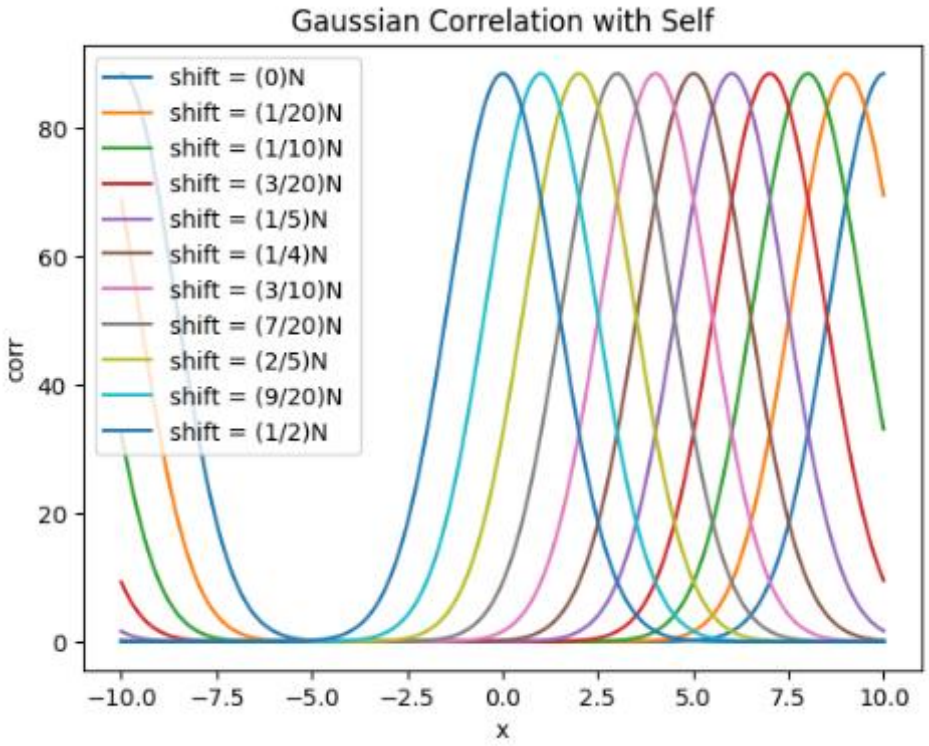

Figure 3. Correlation of a Gaussian with itself shifted by an arbitrary amount

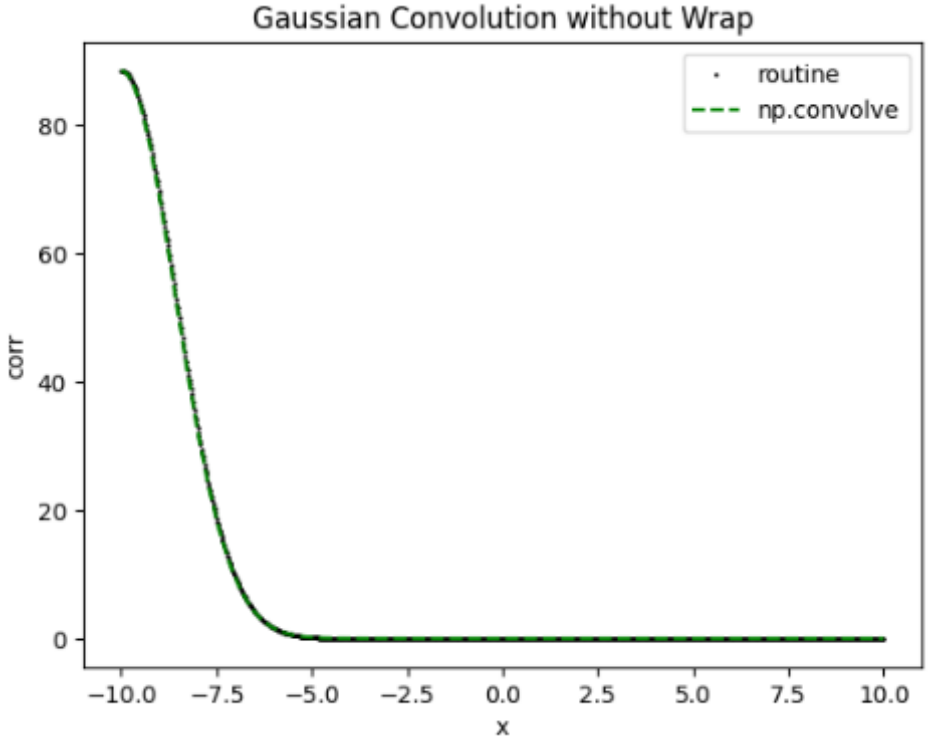

Figure 4. Gaussian convolution without wrap compared to np.convolve equivalent output

4.

a)

Consider the geometric series sum:

$$\sum_{x=0}^{N-1} \alpha^x = \sum_{x=1}^{N} \alpha^{x-1} = \frac{1-\alpha^N}{1-\alpha}$$

Let $[exp\left(\frac{-2\pi ik}{N}\right)]^x = \alpha^x$. Next, substitute $\alpha = exp\left(\frac{-2\pi ik}{N}\right)$.

$$\sum_{x=0}^{N-1} exp\left(\frac{-2\pi ikx}{N}\right) = \frac{1-[exp\left(\frac{-2\pi ik}{N}\right)]^N}{1-\exp\left(\frac{-2\pi ik}{N}\right)} = \frac{1-\exp(-2\pi ik)}{1-\exp\left(\frac{-2\pi ik}{N}\right)}$$

b)

As k →0, the ratio from part (a) becomes 0/0. Hence, apply l'Hospital's rule, by taking the derivatives of the numerator and denominator with respect to k:

$$\lim_{k\to 0} \frac{1-\exp(-2\pi ik)}{1-\exp\left(\frac{-2\pi ik}{N}\right)} = \lim_{k\to 0} \frac{-2\pi i \exp(-2\pi ik)}{\frac{-2\pi i}{N}\exp\left(\frac{-2\pi ik}{N}\right)} = \frac{2\pi i}{\frac{2\pi i}{N}} = N$$

For integer k is a multiple of N, let k=aN.

Substitute Euler's relationship, $\exp(-2\pi ik) = \cos(-2\pi k) + i\sin(-2\pi k)$.

$$\frac{1-\cos(-2\pi k)-i\sin(-2\pi k)}{1-\cos\left(\frac{-2\pi k}{N}\right)-i\sin\left(\frac{-2\pi k}{N}\right)} = \frac{1-\cos(-2\pi k)-i\sin(-2\pi k)}{1-\cos\left(\frac{-2\pi aN}{N}\right)-i\sin\left(\frac{-2\pi aN}{N}\right)} = \frac{1-1-0}{1-\cos(-2\pi a)-i\sin(-2\pi a)} = \frac{0}{1-\cos(-2\pi a)-i\sin(-2\pi a)}$$

If a is an integer (i.e. integer k is a multiple of N), the denominator is zero. For the 0/0 ratio, l'Hospital's rule would apply, and a limit would result in N.

If a is not an integer (i.e. integer k is not a multiple of N), the denominator is non-zero. Thus, **the ratio equals zero.**

c)

A non-integer value of k was selected for the sine wave; the analytic estimate of the DFT was plotted (Figure 5). FFT agreed well with the analytic estimate. The resultant profile was close to that of a delta function, although some spectral leakage observed in the edges, reflected by the curvature of ascent and descent about the putative delta function pulse. Comparison with the in-built np.fft function output evidenced a good agreement to within machine precision, whose residuals could be viewed in Figure 6.

d)

Possibility of leakage minimized was explored via windowing. A proper window was selected as $0.5 - 0.5\cos(2\pi x/N)$. Multiplication by this window resulted in a dramatic decrease in the spectral leakage for the non-integer period sine wave (Figure 7).

e)

FT of the window was shown to equal [N/2, -N/4, 0, …, 0, …, -N/4] numerically. For N=1000, the resultant FFT centered about 0 was noted at [500, -250, 0, …, 0, -250]. Rearrangement thereof about 500 produced [0, …,-250, 500, -250, …, 0]. A windowed FT could accordingly be attained by appropriate combinations of each point in the unwindowed FT and its immediate neighbors. A routine to apply a neighbor-convolved transformation based on the -N/4, +N/2, -N/4 was thereafter constructed. The resultant neighbor-convolved FT in comparison to the previously windowed transformation could be seen in Figure 8. Both methods appeared to produce closely matched outcomes in FT.

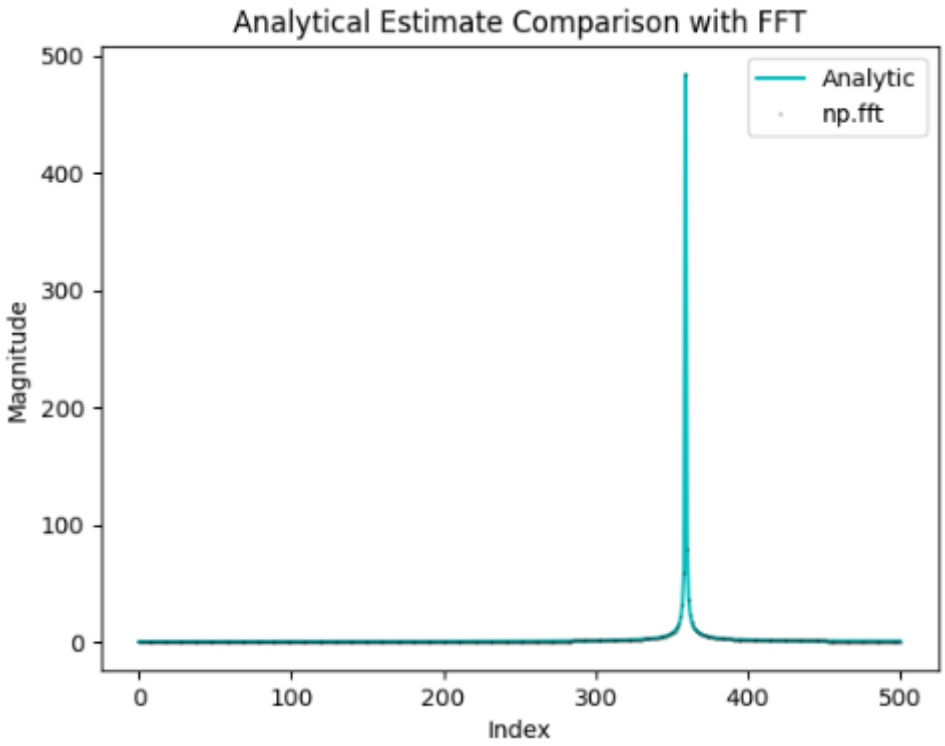

Figure 5. Analytic estimate of FFT compared to output of np.fft

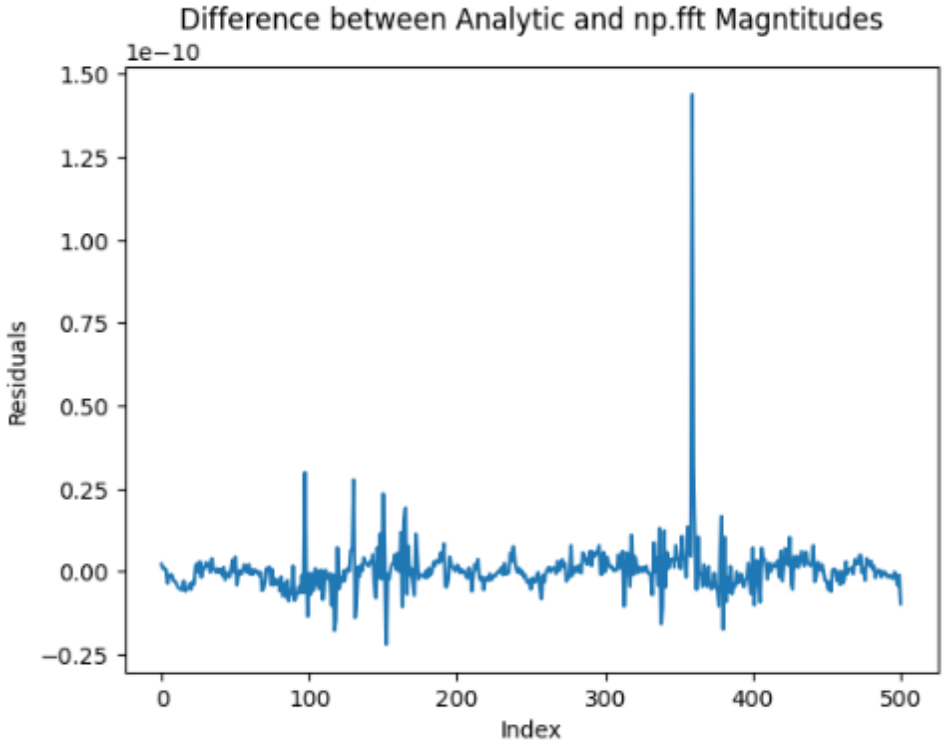

Figure 6. Agreement between analytic and np.fft outputs

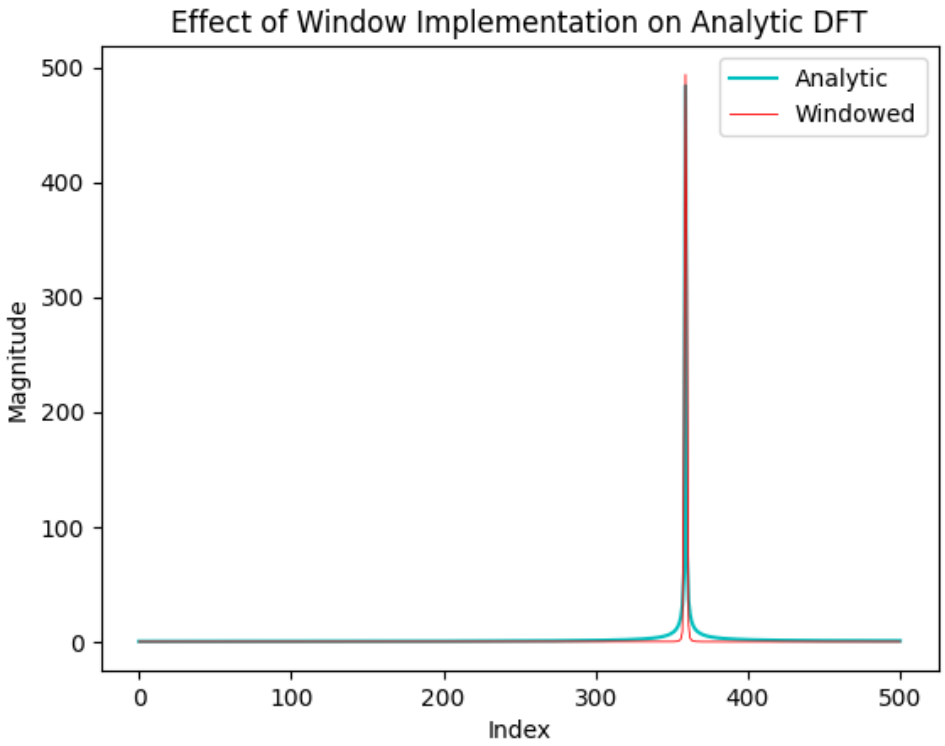

Figure 7. Minimization of spectral leakage in analytic DFT via windowing

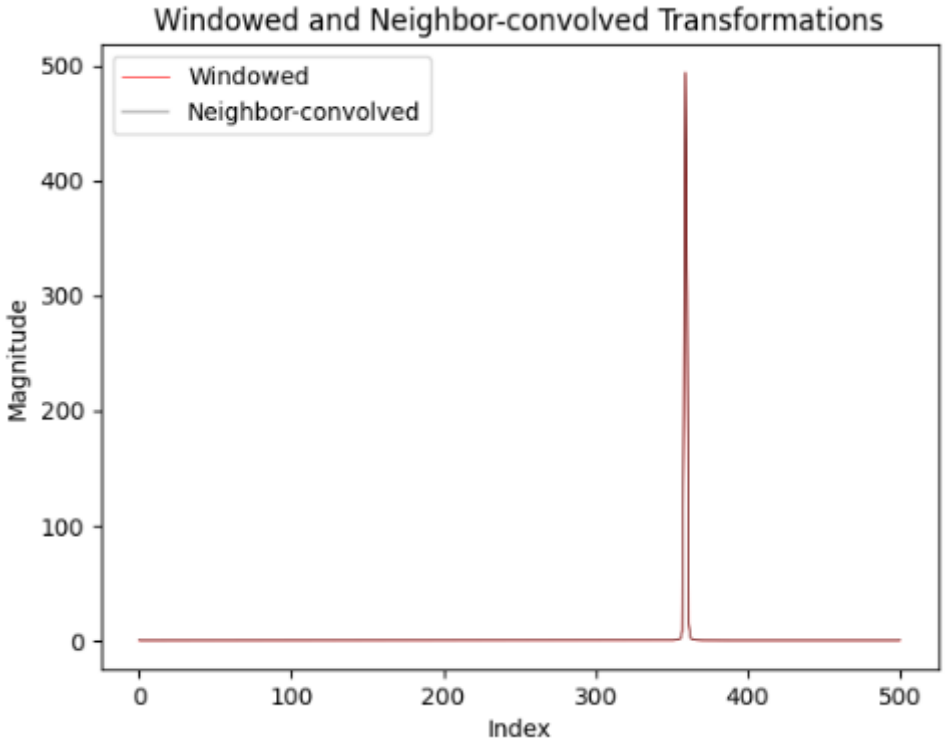

Figure 8. Close agreement between neighbor-convolved and windowed FTs

5.

a)

Noise models for the Hanford (H) and Livingston (L) detectors were constructed separately. Initially, raw data (Figure 9) was acquired and classified according to the LIGO events list (Table 1).

Table 1. Events List Template Match

Template	H/L Trial
GW170	920
GW150	446
LVT	884
GW151	334

Data smoothing required identification of an appropriate window to limit the power spectra to a useful domain. A window with an extended flat period near the center to avoid tapering the data and/or templates, where the signal would not be small, was ideal. A Tukey window (Figure 10) was thus selected to analyze the time-series data so that tapering would be confined in proximity of the edges of the window while full power would be permitted elsewhere.

Square of the magnitude of the FT of windowed raw data generated the power spectra (Figure 11), compelling the removal of undesirable noise. Hence, smoothing was necessary. Function *smooth_vector* was utilized to de-noise the power spectra, utilizing a Gaussian kernel constructed with $\sigma=3$.

According to LIGO, data points with frequencies less than 20Hz and greater than 2000Hz were nonsensible. Below 20 Hz, data would not have been calibrated properly. Since the Nyquist rate is $4096\text{Hz}/2 = 2048$ Hz, the datapoints above 2000Hz would need to be discarded. Thus, the smoothed power spectra were established in the [20Hz, 2000Hz] domain. Subsequent computations were based on this delimited domain, enabling corresponding noise and uncertainty calculations in parts b-f. Resultant spectra presented as much smoother with preserved peaks (Figure 11).

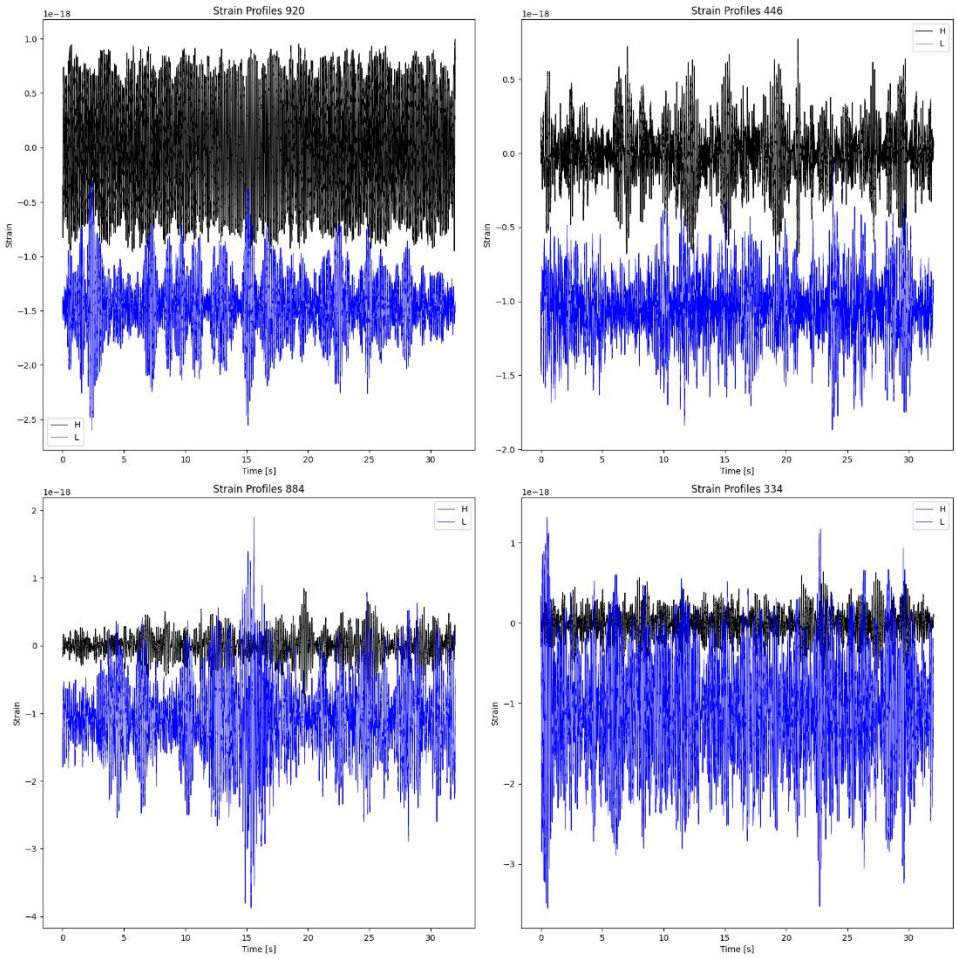

Figure 9. Strain profiles of four trials at stations H and L

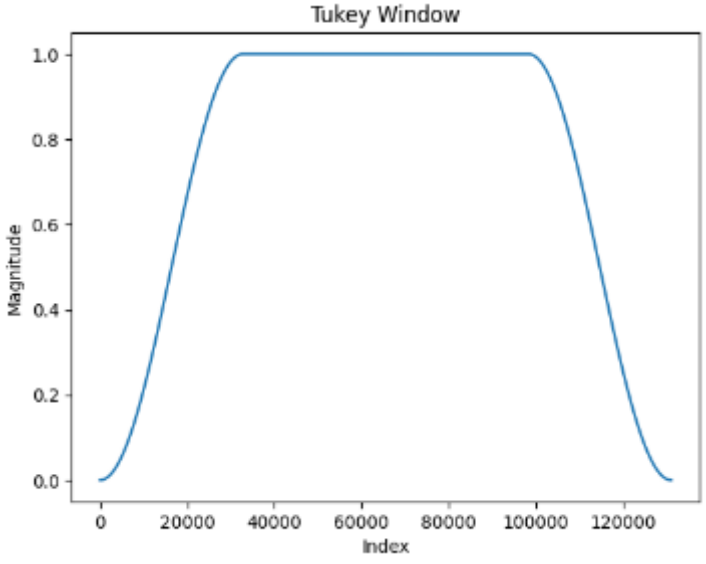

Figure 10. Tukey window profile

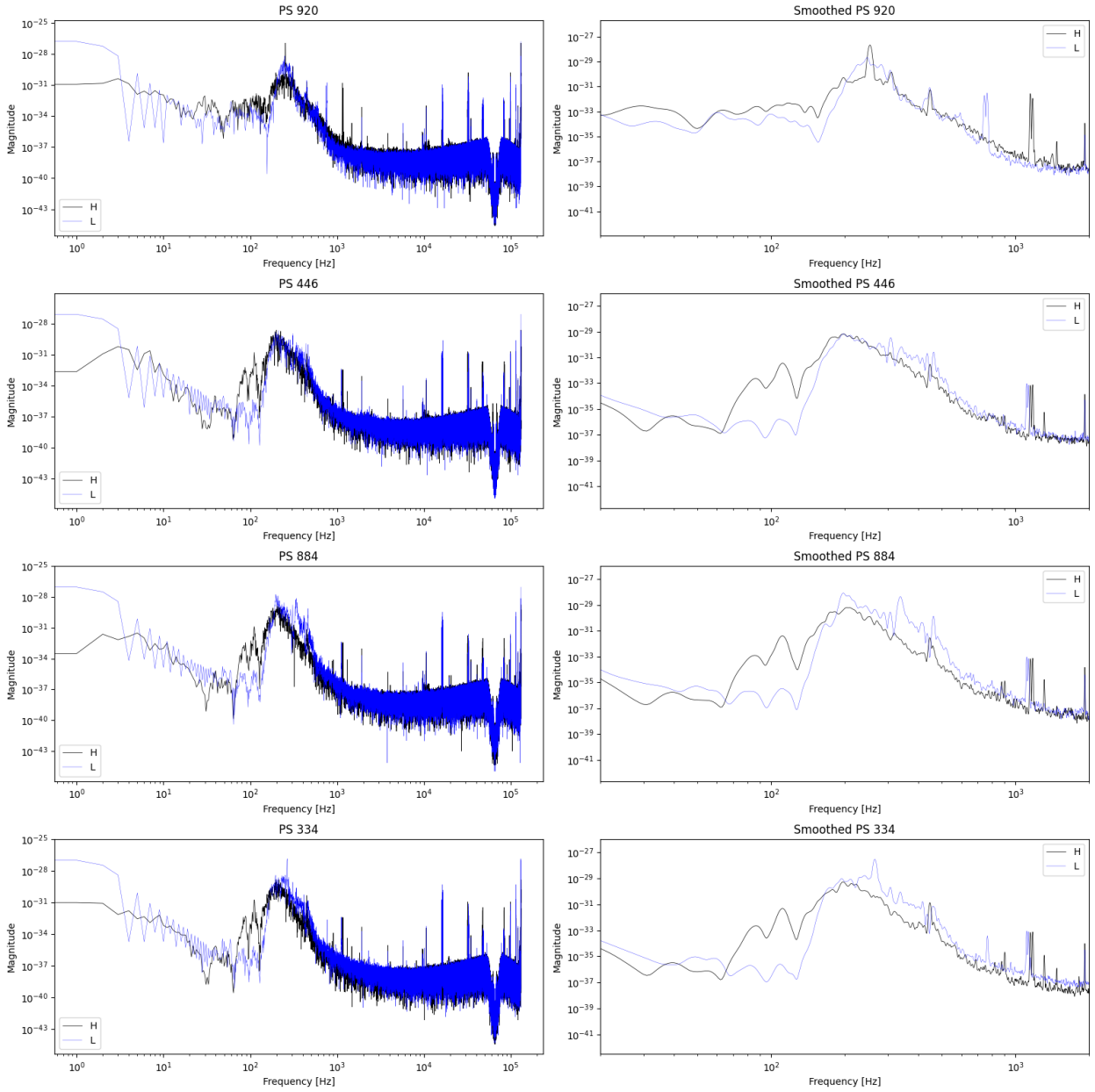

Figure 11. Raw and Smoothed Power Spectra of four trials at H and L stations

The process to construct noise models was concluded upon repetition of the aforementioned steps on the mean power spectra of trials at H and L. The mean power spectra and resultant noise models to be employed in subsequent investigations could be visualized in Figure 12.

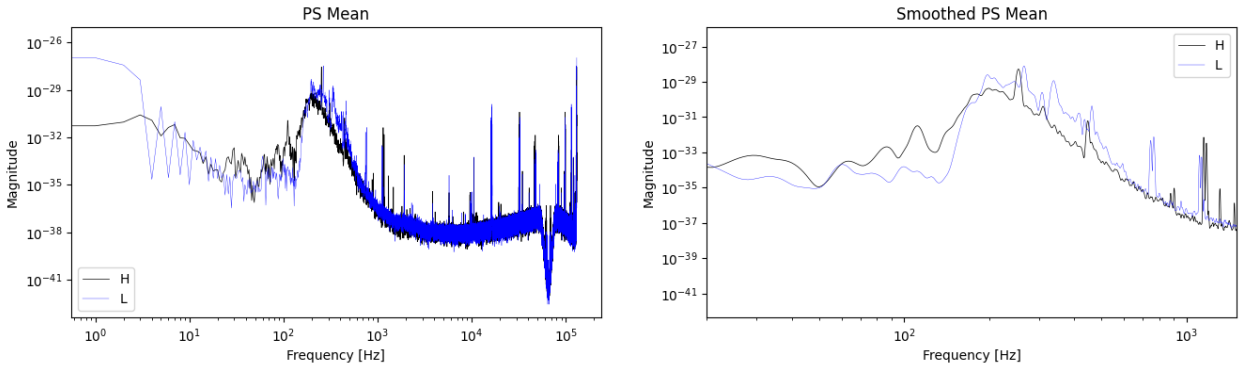

Figure 12. Mean power spectra and noise models

b)

Noise models established in part (a) were subsequently utilized in the match filter investigation with $m(\tau) = A(t-\tau)^T N^{-1} d[A(t-\tau)^T N^{-1} A(t-\tau)]^{-1}$ where template A, noise N, and experimental data d would generate the match parameter m. Since $N^{-1} = (N^{-1/2})^2$:

$$m(\tau) = [N^{-1/2}A(t-\tau)^T][N^{-1/2}d]\{[N^{-1/2}A(t-\tau)^T][N^{-1/2}A(t-\tau)]\}^{-1}$$

where Hessian $H = [N^{-1/2}A(t-\tau)^T][N^{-1/2}A(t-\tau)]$.

Both the data and filters were pre-processed in respect of the designated window. FT thereafter facilitated the computation of the preceding relationship. Whereas T_{white} was the whitened filter, while H_{white} and L_{white} represented the mean whitened strain data from stations H and L. Inverses of discrete FT of real input computed by rfft of $conj(T_{white})*H_{white}$ and $conj(T_{white})*L_{white}$, respectively for H and L, resulted in the matched filter outcomes as shown in Figure 13.

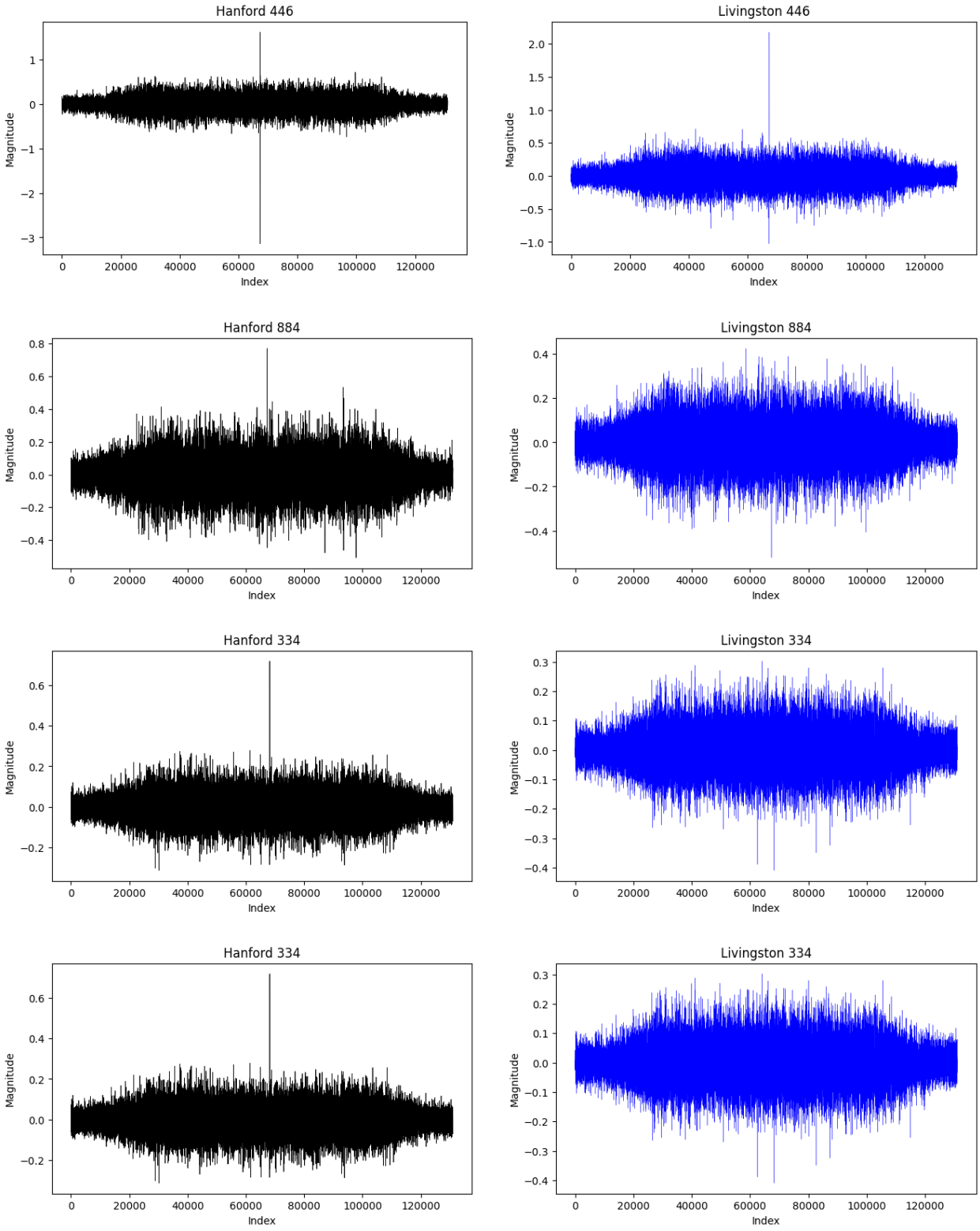

Figure 13. Matched filter outcomes from H and L stations

c)

Signal to Noise Ratio (SNR) for the observations were estimated as the ratio of the signal of greatest magnitude to the standard deviation of the spread for the matched filter data. Hessian assisted in calculation of the analytic SNR, which was based on the ratio of the signal of greatest magnitude to $(H)^{1/2}$ adjusted for size of template.

Combined HL SNRs were also computed. Square of the SNR for the combined HL data should equal the sum of the squares of each trial's SNR. Resultant SNR values are shown in Table 2.

Table 2. SNR Values from Matched Filter Observations and Analytic Calculations

Trial	H	L	Combined HL
Observed			
920	9.78756	10.39028	14.27426
446	18.94175	14.17345	23.65749
884	7.44171	5.69467	9.37061
334	11.06002	6.13425	12.64726
Analytic			
920	9.9768	8.79905	13.30262
446	19.31355	14.77288	24.31566
884	7.37907	5.62539	9.27877
334	10.63241	6.80546	12.62388

d)

The SNR values acquired from the scatter in the matched filter were compared to analytic SNRs. Although on the same order of magnitude, the differences were generally less than 10%. The greatest SNR difference was observed for the L920 trial (~20%). The noise model could be qualified as relatively successful, albeit its over- and under-estimation of the noise was inconsistent between trials as well as across stations. The combined HL SNR values may be more realistic estimates of the expected noises. Further delimitation of the frequency domain (i.e. >20Hz, <2000Hz) might improve the SNR accuracies. Adjustment of the smoothing level could additionally provide insight into the impact of smooth_vector function and its σ parameter on the SNR results.

e)

The frequency from each event, f_H and f_L, where half the weight should come from above that frequency and half below, was determined via a weighted square average of the whitened spectrum of the template of each trial (Table 3). The rationale for this methodology was based on the expectation of how the signal should have appeared such that a mid-range frequency would be selected to partition the total power into two equal components.

Table 3. Half-weight Frequencies

Trial	f_H [Hz]	f_L [Hz]
920	107.82239	120.65234
446	111.97820	123.61566
884	101.69997	115.29871
334	108.80970	126.15353

f)

The time of arrival was determined via the horizontal shift of the matched filter for each trial by identifying the point in time corresponding to the maximum magnitude of signal strength at each station. The difference therebetween was identified as the time of arrival difference Δt for each trial, comparison of which enabled the computation of the positions of gravitational wave events. A crow's distance between two stations, d_{crow} was set at 3041.1 km. Based on the speed of light c= 2.998×10^8 m/s, an approximation of the angular uncertainty δ_θ could be determined as per Figure 14.

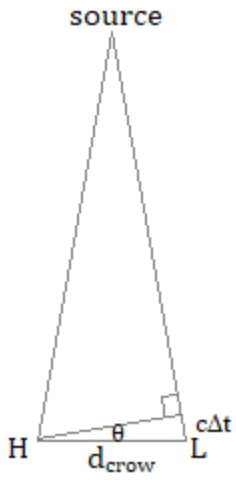

Figure 14. Geometric relationship between interstation distance and angular position

t_i	time increment in measurement	0.00024414	[s]
δ_t	uncertainty in time detection	$(20)(2)^{1/2}(t_i)=0.00690534$	[s]
θ	angular position	$\sin^{-1}(c\Delta t/d_{crow})$	[rad]
δ_θ	angular uncertainty	$(c\delta_t/d_{crow})(1-(c\Delta t/d_{crow})^2)^{-1/2}$	[rad]

Resultant Δt and θ values are shown in Table 4.

Table 4. Signal Arrival Time Differences and Estimated Angular Positions

Trial	Δt [s]	θ [rad]
HL920	0.10156	0.31823
HL446	0.23438	0.80675
HL884	0.01562	0.04815
HL334	0.03906	0.12063

The typical positional uncertainty expected due to a few thousand km apart stations was on the **order of 10^0 rad**. The mean time difference and angular position as well as corresponding uncertainties were:

$\Delta t = 0.00305 \pm 0.00691$ s

$\theta = 0.32344 \pm 0.88400$ rad